

# Low temperature structural transition in $\text{FeCr}_2\text{S}_4$

M. Mertinat,<sup>1</sup> V. Tsurkan,<sup>1,2</sup> D. Samusi,<sup>2</sup> R. Tidecks,<sup>1</sup> and F. Haider<sup>1</sup>

<sup>1</sup>Institut für Physik, Universität Augsburg, D-86135 Augsburg, Germany

<sup>2</sup>Institute of Applied Physics, Academy of Sciences of Moldova, MD 2028 Chisinau, R. Moldova  
(Dated: December 6, 2020)

Transmission electron microscopy studies of [110] and [111] oriented  $\text{FeCr}_2\text{S}_4$  single crystals at different temperatures reveal a structural transition at low temperatures indicating a cubic-to-triclinic symmetry reduction within crystallographic domains. The overall crystal symmetry was found to be reduced from  $Fd\bar{3}m$  to  $F43m$ . The triclinic distortions were suggested to result from the combined actions of tetragonal distortions due to the Jahn-Teller active  $\text{Fe}^{2+}$  ions and trigonal distortions due to a displacement of the  $\text{Cr}^{3+}$  ions in the h111i direction.

PACS numbers: 75.50.Pp; 61.14.Lj; 61.50.Ks

Spin-lattice coupling in highly correlated magnetic systems plays an important role in the formation of the magnetic ground state and governs the electronic properties. Electron-phonon interaction and lattice polarons contribute essentially to the colossal magnetoresistance (CMR) effect and the magnetic field induced metal-insulator transition in manganite perovskites [1, 2]. In addition to small lattice polarons, correlated lattice distortions may appear and result in nanoscale regions with charge and orbital order [3]. These regions are connected with the change of the structural symmetry and are also responsible for the magnetotransport anomalies.

In this letter we report the observation of a structural lattice transformation at low temperatures in another CMR material, ternary ferrimagnetic  $\text{FeCr}_2\text{S}_4$  with a cubic spinel-type crystal structure [4]. The existence of local structural distortions and the possibility of a structural transformation in this compound was suggested already in 1967 based on the appearance of quadrupole splitting and a low temperature anomaly of the electric field gradient induced on the tetrahedrally coordinated  $\text{Fe}^{2+}$  ions [5, 6]. These features were attributed to a strong coupling between the Jahn-Teller (J-T) active ferrous ions which allows a distortion of the  $\text{FeS}_4$  tetrahedrons [7] and were explained in the framework of static and dynamic J-T effects. An alternative explanation suggested another type of orbital ordering due to a hybridization of Cr and Fe states [8]. The interpretation of the Möbauer data, however, was in conflict with X-ray and neutron scattering diffraction investigations, which found that polycrystalline  $\text{FeCr}_2\text{S}_4$  remains a cubic spinel down to 4.2 K [9, 10]. In powdered single crystals, the symmetry was found to be unchanged, too, although a broadening of the X-ray diffraction lines was observed and was suggested as due to inhomogeneous lattice distortions below the Curie temperature down to 4.2 K [11].

Several recent experimental investigations on  $\text{FeCr}_2\text{S}_4$  single crystals pointed out the importance of a spin-lattice coupling. A cusp-like anomaly in the temperature dependence of the magnetization at  $T_m \approx 60$  K and a splitting of zero-field cooled and field cooled magnetiza-

tion below this temperature was observed [12]. Hydrostatic pressure investigations [13] show that the magnetic anomaly at  $T_m$  in  $\text{FeCr}_2\text{S}_4$  is strongly sensitive to lattice contraction.  $T_m$  is increased by pressure with a rate of  $dT_m/dp \approx 30$  K/GPa. This behavior was related to the appearance of a non-cubic magnetocrystalline anisotropy due to structural distortions. AC-susceptibility measurements [14] and magnetoresistance studies [13] indicate that the spin-glass-like features below  $T_m$  are connected with changes in the domain structure due to additional pinning centers which were suggested to appear as a result of a structural lattice transformation. Very recently ultrasonic measurements of  $\text{FeCr}_2\text{S}_4$  single crystals gave evidence for a structural transformation at  $\approx 60$  K. The elastic moduli manifest a step-like feature around this temperature indicating a structural phase transition of first-order type. Below 60 K a pronounced softening of the elastic moduli was found. The experimental data indicate the appearance of a trigonal distortion which was explained in terms of an orbital ordering with coupling of the orbitals of Fe ions along the h111i direction [15].

To investigate the structural distortions we used selected area electron diffraction (SAED) in a transmission electron microscope (TEM). It shows a cut through the reciprocal lattice and, therefore, is very sensitive to small changes of the local crystal symmetry of the lattice [16]. Any changes in the crystal symmetry and the lattice constants can thus be directly observed.

Ternary polycrystalline material obtained by solid state reaction from high purity elements was the source to grow  $\text{FeCr}_2\text{S}_4$  single crystals by chemical transport reaction [17]. Chromium chloride and tellurium chloride were used as the source of the transport agent,  $\text{Cl}_2$ . The growth temperature was varied between 820 and 850 C. The resulting crystals grew to a size up to 4-6 mm. The single phase spinel structure was confirmed by X-ray diffraction analysis. Sample composition was checked by electron probe microanalysis, which revealed a nearly stoichiometric composition (within 2 mole%) and a small amount of chlorine (0.5 mole%). Plates cut from single crystals in different directions were glued on a Cu sup-

porting disc with a 800  $\mu\text{m}$  diameter centered hole. After mechanical dimpling, the samples were thinned using an Ar<sup>+</sup> ion polishing system. The TEM (Philips CM 12 operating at 120 kV) was assembled with a low temperature cooling stage. The double tilt sample holder, Gatan 636LHe, was cooled with liquid helium to a lowest temperature of 14 K. The diffraction images were recorded in situ for different temperatures. The microscope parameters were kept unchanged for a series of diffraction images in order to minimize possible errors due to hysteresis effects of the magnetic electron lenses. The accuracy of the temperature measurement was better than 3 K. The images were recorded with a CCD camera or negative film plates which were digitized for further processing.

To evaluate the SAED patterns and determine the spot positions a special computer algorithm was developed [18]. The distances and angles between neighboring spots were calculated and averaged. The distances in the diffraction patterns,  $l_i$ , were transformed into interplanar spacings in direct space,  $d_i$ . Relative changes less than  $10^{-4}$  can be detected. To construct the unit cell, samples with two different orientations ([110] and [111]) are needed. In the cubic structure, for the [110] orientation the diffraction pattern should exhibit two equal angles (noted  $\phi_1 = \phi_2 = 54.7^\circ$  in Fig. 1a) and a third one,  $70.6^\circ$ . From the three distances between the spots two must be equal (noted as  $l_1$  and  $l_2$  in Fig. 1a) and differ from the third one ( $l_3$ ). The ratio  $l_1/l_3 = l_2/l_3 = 1:1.5$ . In the diffraction pattern of an ideal fcc crystal in [111] direction all distances between the neighbored spots are equal and all angles between these spots are  $60^\circ$  [16].

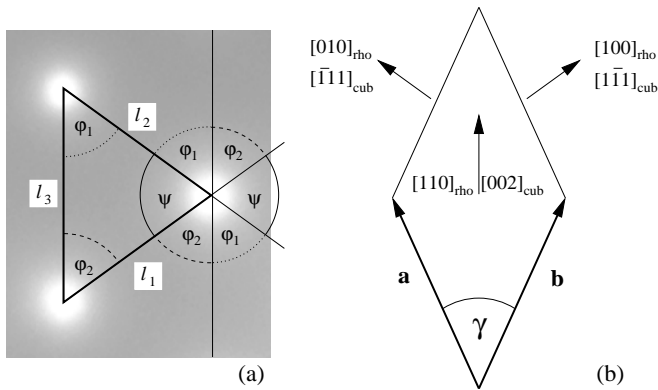


FIG. 1: (a) SAED pattern of [110] zone axis orientation with the triangle used for evaluation of distances and angles; (b) [001] view of rhombohedral primitive cell with the cubic and rhombohedral directions.

Figures 2a and b show a high resolution image and SAED pattern of the  $\text{FeC}_2\text{S}_4$  single crystal in [110] zone axis orientation. The image indicates a quite regular lattice structure without defects such as precipitates and

dislocations (Fig. 2a). The corresponding diffraction pattern shows the ordinary reflections (000) and (111), but also the (002) reflection which is forbidden for the  $Fd\bar{3}m$  space group (Fig. 2b). It was observed in all sample regions with different thicknesses at all temperatures. To verify whether this is an intrinsic reflection or is caused by double diffraction we performed TEM investigations on a sample with [100] orientation. For this orientation no contribution from double diffraction is allowed. Indeed, for [100] oriented samples we also observed small but clearly pronounced (200) reflections (Fig. 2c). Our results are similar to that observed in  $\text{MgAl}_2\text{O}_4$  spinel with reduced symmetry [19] and suggest that the space group of  $\text{FeC}_2\text{S}_4$  is  $F43m$  rather than  $Fd\bar{3}m$ .

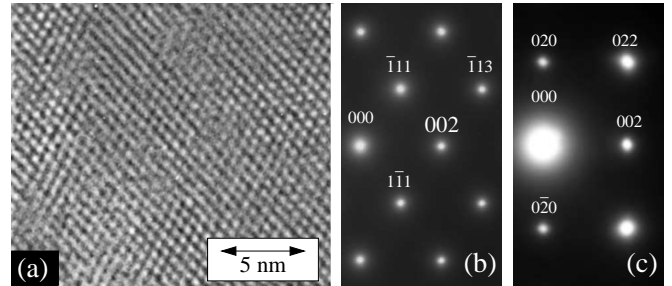


FIG. 2: (a) High resolution image of [110] $\{\text{FeC}_2\text{S}_4$ . (b) SAED pattern of [110] and (c) [100] oriented samples.

In Fig. 3 the temperature dependence of the diffraction pattern parameters are shown for the [111] oriented sample. Above 60 K the angles and spacings are equal, as expected for a fcc crystal. Below, a noticeable difference between the angles appears (Fig. 3a), whereas the interplanar spacings (Fig. 3b) show a less pronounced deviation. For the [110] orientation we observed three different types of behavior of the diffraction pattern parameters for different sample positions, noted below as types A, B and C. For the A-type patterns the parameters are shown in Fig. 3c and d. Below about 50 K clear differences between angles  $\phi_1$  and  $\phi_2$  (Fig. 3c) and spacings  $d_1$  and  $d_2$  (Fig. 3d) are found. The values of  $\phi_1$  and  $d_2$  increase, whereas  $\phi_2$  and  $d_1$  decrease for decreasing temperature. The third parameters ( $\psi$  and  $d_3$ ) also show a clear increase and decrease, respectively. The B-type pattern is also characterised by a splitting of  $\phi_1$  and  $\phi_2$ , and  $d_1$  and  $d_2$  below 50 K [20], but with an opposite and less pronounced variation compared to type A. For the C-type behaviour no splitting or other significant changes of the diffraction parameters were observed. Figure 4 and Tab. 1 summarize the experimental observations of these three different types of behavior. The variation of  $\psi$  and  $d_3$  versus the splitting between  $\phi_1$  and  $\phi_2$  with temperature is presented in Fig. 4a and b, respectively.

To understand the results, we computed the diffraction patterns for different symmetry types of the unit cell. As a starting point for the fitting procedure a primitive

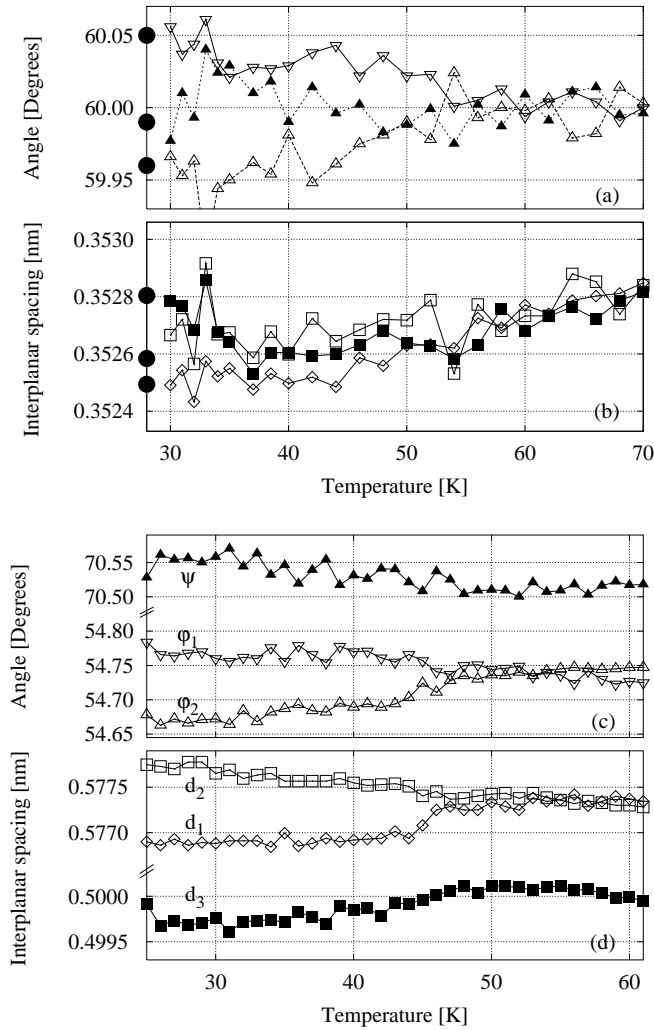


FIG. 3: Angle and interplanar spacing of the diffraction patterns as function of temperature of [111] (a and b) and [110] (c and d) oriented  $\text{FeCr}_2\text{S}_4$ . Full dots: Calculated values for the low-temperature structure.

Type	$\psi$ [°]	$\phi_1$ [°]	$d_{1,2}$ [nm]	$d_3$ [nm]
A	+0.102 (18)	+0.050 (11)	0.00060 (16)	0.00037 (9)
B	0.086 (17)	0.007 (15)	+0.00027 (23)	+0.00024 (7)
C	0.026 (17)	0.009 (11)	+0.00005 (13)	0.00000 (7)

TABLE I: Splitting of the diffraction pattern parameters for the different types in [110] $\{\text{FeCr}_2\text{S}_4$ .

rhombic unit cell was used with the lattice parameters  $a = b = c = 2^{1/2} a_{\text{cub}}$  and  $\alpha = \beta = \gamma = 60^\circ$ , where  $a_{\text{cub}}$  is the lattice constant of the cubic unit cell [21]. The arrangement of the vectors normal to the base planes (as shown in Fig. 1b) directly corresponds to the triangular configuration of the diffraction pattern. The symmetry of the distorted rhombic unit cell is lowered to triclinic.

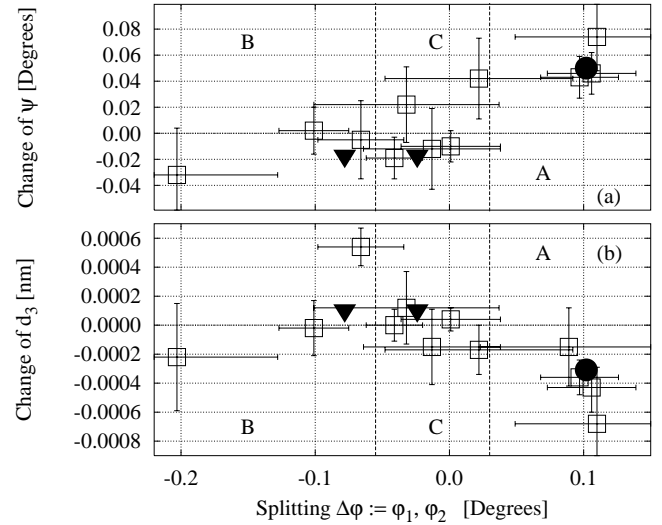


FIG. 4: Variation of the diffraction pattern parameters of [110] $\{\text{FeCr}_2\text{S}_4$ . Symbols: See text.

The parameters  $c$ , and  $\alpha$  of the triclinic cell were kept constant in the simulation because for the [110] zone axis changes in the [110] direction cannot be detected. Fitting of the type A diffraction pattern data (full dots in Fig. 4) results in  $a = 0.7075(2) a_{\text{cub}}$ ;  $b = 0.7066(2) a_{\text{cub}}$ ;  $c = 0.7071 a_{\text{cub}}$ ;  $\alpha = \beta = \gamma = 60^\circ$ ;  $\alpha = 60.04(1)^\circ$ . Using this crystallographic data the expected changes for the other two types of patterns were calculated assuming that they are related to the other two cubic h110i orientations. The results for that case are marked by full triangles in Fig. 4 and reproduce quite well the experimental data. In the same way, we calculated the expected variations for the [111] zone axis orientation (full dots in Fig. 3a and b) and obtained a very reasonable agreement with the experimental data. This consistency suggests that the three different types of diffraction patterns observed are connected with the creation of different structural domains or twinning planes. The orientation of these special domains alternate between the three h110i directions which were equivalent before transition. The size of these domains was estimated from the lateral sample drift during the experiment to lie between 15 and 50 nm.

To get the difference in the diffraction patterns for the cubic and the triclinic cell we calculated the powder diffraction patterns using the EMS (electron microscopy in a simulation) program by P. Stadelmann [22], yielding changes on the order of  $5 \times 10^{-4}$ . Such small changes can hardly be detected by ordinary X-ray or neutron diffraction where for polycrystalline samples a broadening of the peaks rather than a splitting is observed [9, 10, 11].

Concerning the nature of the structural anomaly in  $\text{FeCr}_2\text{S}_4$ , several mechanisms may be considered. Earlier theoretical [23, 24, 25, 26] and experimental studies [27, 28, 29] of a structural transition in transition

metal oxide spinels attributed them mainly to the Jahn-Teller (JT) active  $\text{Fe}^{2+}$  ions which stabilize the tetragonal phase. In addition the octahedral  $\text{Cr}^{3+}$  ions may contribute to the elastic anisotropy. Depending on the relative strength of the competing effects, a resulting low-temperature tetragonal or orthorhombic structure is established [26, 30]. None of these structures, however, fits our experimental data [18].

From our observations of the reduction of the overall symmetry from  $Fd\bar{3}m$  to  $F43m$  an additional distortion of the octahedral sites can be inferred. A similar reduction of the symmetry was observed in several spinel compounds [29, 31] and was attributed to a displacement of the octahedral-site cations from the center of the octahedron along the  $h111i$  direction producing a trigonal distortion. The presence of trigonal distortions in  $\text{FeCr}_2\text{S}_4$  was also revealed by ultrasonic experiments [15]. Therefore, the observed triclinic distortions in our  $\text{FeCr}_2\text{S}_4$  crystal may result from the combined action of a tetragonal distortion due to tetrahedral-site JT  $\text{Fe}^{2+}$  ions and a trigonal one due to octahedral-site  $\text{Cr}^{3+}$  ions. Since the structural transformation in  $\text{FeCr}_2\text{S}_4$  occurs below the cusp-like anomaly in the magnetization at  $T_m$ , and keeping in mind the strong magnetic crystalline anisotropy in  $\text{FeCr}_2\text{S}_4$  [32, 33] there is probably a contribution from spin-orbital coupling to the lattice distortions. In fact, recent specific heat [34] and ultrasonic studies [15] attributed the low-temperature anomalies in this compound to the orbital degrees of freedom. The structural transformation may result from an orbital ordering. However, the coupling of the orbitals appears to be more complicated than the simple trigonal or tetragonal arrangements suggested in earlier studies [13, 15, 35].

In conclusion, we investigated the crystal structure of the  $\text{FeCr}_2\text{S}_4$  magnetic spinels by SAED. We found a structural anomaly below 60 K which we interpret in terms of a triclinic distortion within crystallographic domains. In addition we found a (200) reflection which indicates that the crystal symmetry belongs to the  $F43m$  symmetry group. Thus, our study clarifies the long standing problem of the structural anomaly in  $\text{FeCr}_2\text{S}_4$ .

---

Electronic address: MarkusMertinat@Physik.uni-Augsburg.DE

- [1] A. J. Millis, P. B. Littlewood, and B. I. Shraiman, *Phys. Rev. Lett.* 74, 5144 (1995).  
 [2] A. J. Millis, B. I. Shraiman, and R. M. Ueller, *Phys. Rev. Lett.* 77, 175 (1996).

- [3] P. Dai et al., *Phys. Rev. Lett.* 85, 2553 (2000).  
 [4] A. P. Ramirez, R. J. Cava, and J. K. Rajewski, *Nature* 386, 156 (1997).  
 [5] M. Eibschutz, S. Shtrikman, and Y. Tenenbaum, *Phys. Letters* 24A, 563 (1967).  
 [6] M. R. Spender and A. H. Morrish, *Solid State Commun.* 11, 1417 (1972).  
 [7] L. F. Feiner, *J. Phys. C* 15, 1515 (1982).  
 [8] L. Brossard et al., *Phys. Rev. B* 20, 2933 (1979).  
 [9] G. Shirane, D. E. Cox, and S. J. Pickard, *J. Appl. Phys.* 35, 954 (1964).  
 [10] C. Brouettes Colombinas, R. Ballestracci, and G. Roult, *J. Phys. (Paris)* 25, 526 (1964).  
 [11] H. Gobel, *J. Magn. Mater.* 3, 143 (1976).  
 [12] V. Tsurkan et al., *Physica B* 296, 301 (2001).  
 [13] V. Tsurkan et al., *J. Appl. Phys.* 90, 875 (2001).  
 [14] V. Tsurkan et al., *J. Appl. Phys.* 90, 4639 (2001).  
 [15] D. Mauer et al., *J. Appl. Phys.* 93, 9173 (2003).  
 [16] L. Reimer, ed., *Transmission Electron Microscopy* (Springer-Verlag, Berlin, 1993), 3rd ed.  
 [17] H. Schäfer, ed., *Chemische Transportreaktionen* (Verlag Chemie, 1962).  
 [18] M. Mertinat, Ph.D. thesis, Universität Augsburg (2003).  
 [19] L. Hwang, A. H. Heuer, and T. E. Mitchell, *Philos. Mag.* 28, 241 (1973).  
 [20] The difference in the detected transition temperature for samples with [110] and [111] orientations may be explained as due to heating of the sample by the electron beam and temperature gradient.  
 [21] E. W. Gorter, *Philips Res. Rep.* 9, 295 (1954).  
 [22] P. A. Stademann, *Ultramicroscopy* 21, 131 (1987).  
 [23] J. B. Goodenough and A. L. Loeb, *Phys. Rev.* 98, 391 (1955).  
 [24] J. D. Dunitz and L. E. Orgel, *J. Phys. Chem. Solids* 3, 20 (1957).  
 [25] P. J. Wojtowicz, *Phys. Rev.* 116, 32 (1959).  
 [26] J. B. Goodenough, *J. Phys. Chem. Solids* 25, 151 (1964).  
 [27] M. H. Francombe, *J. Phys. Chem. Solids* 3, 37 (1957).  
 [28] R. J. A. Mott, A. Wold, and D. B. Rogers, *J. Phys. Chem. Solids* 25, 161 (1964).  
 [29] A. Wold et al., *J. Appl. Phys.* 34, 1085 (1963).  
 [30] S. Krupicka, *Physik der Ferrite und verwandten magnetischen Oxide* (Vieweg, Braunschweig, 1973).  
 [31] N. W. Grimes, *Philos. Mag.* 26, 1217 (1972).  
 [32] R. P. van Stapelle, J. S. van Wieringen, and P. F. Bongers, *J. Phys. C* 32, 53 (1971).  
 [33] L. Goldstein, P. Gibard, and L. Brossard, in *Magnetism and Magnetic Materials. 21th Ann. Conference - Philadelphia* (1976), pp. 405-407.  
 [34] V. Tsurkan et al., to be published.  
 [35] We exclude defects as a reason of distortions because, as show our studies on  $\text{Fe}_{1-x}\text{Cr}_x\text{S}_4$  single crystals, the lower temperature anomaly at 60 K is present in the magnetization of stoichiometric as well as for Fe deficient and Fe excess samples (to be published).